

Ultrafast Spectroscopy of $[\text{Mn}(\text{CO})_3]$ Complexes: Tuning the Kinetics of Light-Driven CO Release and Solvent Binding

Wade C. Henke,[#] Christopher J. Otolski,[#] William N. G. Moore, Christopher G. Elles,^{*} and James D. Blakemore^{*}



Cite This: *Inorg. Chem.* 2020, 59, 2178–2187



Read Online

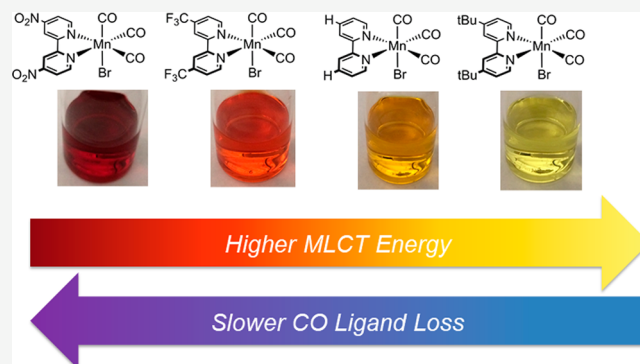
ACCESS |

Metrics & More

Article Recommendations

Supporting Information

ABSTRACT: Manganese tricarbonyl complexes are promising catalysts for CO_2 reduction, but complexes in this family are often photosensitive and decompose rapidly upon exposure to visible light. In this report, synthetic and photochemical studies probe the initial steps of light-driven speciation for $\text{Mn}(\text{CO})_3(^R\text{bpy})\text{Br}$ complexes bearing a range of 4,4'-disubstituted 2,2'-bipyridyl ligands (^Rbpy , where $R = ^t\text{Bu}$, H, CF_3 , NO_2). Transient absorption spectroscopy measurements for $\text{Mn}(\text{CO})_3(^R\text{bpy})\text{Br}$ coordination compounds with $R = ^t\text{Bu}$, H, and CF_3 in acetonitrile reveal ultrafast loss of a CO ligand on the femtosecond time scale, followed by solvent coordination on the picosecond time scale. The $\text{Mn}(\text{CO})_3(^{\text{NO}_2}\text{bpy})\text{Br}$ complex is unique among the four compounds in having a longer-lived excited state that does not undergo CO release or subsequent solvent coordination. The kinetics of photolysis and solvent coordination for light-sensitive complexes depend on the electronic properties of the disubstituted bipyridyl ligand. The results indicate that both metal-to-ligand charge-transfer (MLCT) and dissociative ligand-field (d-d) excited states play a role in the ultrafast photochemistry. Taken together, the findings suggest that more robust catalysts could be prepared with appropriately designed complexes that avoid crossing between the excited states that drive photochemical CO loss.



INTRODUCTION

Manganese tricarbonyl complexes of the form $\text{Mn}(\text{CO})_3(^R\text{bpy})\text{Br}$ ($^R\text{bpy} = 4,4'$ -disubstituted 2,2'-bipyridyl) are promising catalysts for the conversion of carbon dioxide (CO_2) into carbon monoxide (CO) and/or formate, valuable precursors to chemical feedstocks and commodity chemicals.^{1,2} The synthetic chemistry for the manganese complexes was developed by Wilkinson and co-workers³ and later extended by Wrighton, Meyer, and others.⁴ These complexes are remarkable for their ease of preparation and can be synthesized from commercially available or readily prepared ligands, ^Rbpy , and the synthon $\text{Mn}(\text{CO})_5\text{Br}$. Similar synthetic chemistry and catalytic properties have been demonstrated with analogous rhenium tricarbonyl complexes, $\text{Re}(\text{CO})_3(^R\text{bpy})\text{Br}$, which were investigated for catalysis much earlier by the groups of Lehn⁵ and Meyer,⁶ and popularized by the groups of Fujita,⁷ Kubiak,⁸ Ishitani,⁹ and others.¹⁰ However, considering the significantly greater abundance of manganese, many research groups have continued to develop new $[\text{Mn}(\text{CO})_3]$ -based catalysts. These efforts have led to a remarkable flourishing of reports showing that a variety of bidentate ligands can support and/or tune the electronic, photophysical, and catalytic properties of $[\text{Mn}(\text{CO})_3]$ complexes.^{11–13}

A defining feature that distinguishes the rhenium complexes from their manganese analogues is markedly better stability upon irradiation with visible light.¹⁴ Importantly, many $[\text{Mn}(\text{CO})_3]$ complexes are susceptible to speciation¹⁵ and/or degradation¹⁶ upon exposure to visible light. For example, our preliminary investigations in organic solvents revealed that $\text{Mn}(\text{CO})_3(^R\text{bpy})\text{Br}$ complexes begin to decompose within minutes under ambient fluorescent lighting, as is evident from peak broadening in the ^1H NMR spectra. A review describing the photochemistry of a variety of metal carbonyl species provides context to the light sensitivity of $\text{Mn}(\text{CO})_3(^R\text{bpy})\text{Br}$ in solution.¹⁷ Specifically, the light sensitivity of many first-row transition-metal complexes is often a consequence of the inherent excited-state electronic structure of the compounds. However, because the light sensitivity of the $\text{Mn}(\text{CO})_3(^R\text{bpy})\text{Br}$ complexes presents a potential challenge to their use in electrochemical or, especially, photoelectrochemical systems

Received: September 16, 2019

Published: January 28, 2020

for CO_2 conversion, we became interested in the underlying processes that contribute to speciation and/or degradation.

Separate from their role as catalysts, the light-induced reactivity of manganese complexes makes the $[\text{Mn}(\text{CO})_3]$ moiety a promising motif for developing a relatively new class of putative therapeutics known as photoinduced CO-releasing molecules (photo-CORMs).¹⁸ Classic work on the photochemical properties of dimanganese decacarbonyl ($[\text{Mn}(\text{CO})_5]_2$) revealed the susceptibility of low-valent manganese complexes to release CO under irradiation with visible light.^{19,20} However, $[\text{Mn}(\text{CO})_5]_2$ absorbs only very weakly in the visible region, which is problematic from the standpoint of therapeutic development because UV light does not readily penetrate the skin.²¹ The need for the efficient activation of photo-CORMs at longer wavelengths has motivated the development of novel $[\text{Mn}(\text{CO})_3]$ -based compounds that absorb light in the visible region. Toward this goal, Schatzschneider and co-workers developed the first $[\text{Mn}(\text{CO})_3]$ -based photo-CORMs supported by various tripodal ligands.²² Further work by several research groups has led to numerous platforms and ligand systems in this family that allow effective photoinduced CO release.²³ Notably, Mascharak and co-workers highlighted the light sensitivity of $\text{Mn}(\text{CO})_3(^{\text{R}}\text{bpy})\text{Br}$ complexes, demonstrating that $\text{Mn}(\text{CO})_3(^{\text{H}}\text{bpy})\text{Br}$ is capable of visible-light-induced CO release at 420 nm.²⁴

Despite the potential role of $\text{Mn}(\text{CO})_3(^{\text{R}}\text{bpy})\text{Br}$ complexes in diverse applications ranging from catalysis to phototherapeutics, the photophysical properties of these compounds have received surprisingly little attention. The analogous $[\text{Re}(\text{CO})_3]$ complexes have been studied with nanosecond and femtosecond transient absorption (TA) spectroscopy, as well as time-resolved IR absorption measurements.^{25,26} Vlček and co-workers, in particular, have examined various aspects of the ligand-dependent excited-state behavior of $[\text{Re}(\text{CO})_3]$ complexes bearing diimine-type ligands, providing important insights into electron-transfer behavior and the resulting chemical reactivity.^{27,28} However, to the best of our knowledge, no femtosecond or picosecond pump–probe experiments have examined the fundamental photochemistry of $[\text{Mn}(\text{CO})_3]$ complexes bearing diimine ligands. Only steady-state experiments involving spectroscopic characterization of the products following bulk photolysis¹⁵ and a nanosecond pulse radiolysis study of the reduction-induced reactivity of $\text{Mn}(\text{CO})_3(^{\text{tBu}}\text{bpy})\text{Br}$ have been reported.²⁹

In this contribution, we examine the fundamental photochemistry of $\text{Mn}(\text{CO})_3(^{\text{R}}\text{bpy})\text{Br}$ complexes with disubstituted ligands bearing *tert*-butyl (1), hydridyl (2), trifluoromethyl (3), and nitro (4) groups (Chart 1) following exposure to visible light. Ultrafast TA spectroscopy reveals the loss of a CO ligand on the femtosecond time scale, followed by solvent coordination on the picosecond time scale for 1–3 in acetonitrile (MeCN). The kinetics of these reactions depend on the identity of the substituents at the 4 and 4' positions of the ^Rbpy ligand and correlate well with the Hammett

parameters associated with the substituent groups. In contrast with the results for 1–3, TA spectroscopy and gas chromatography (GC) measurements indicate that 4 does not undergo CO release. Taken together, these observations implicate metal-to-ligand charge-transfer (MLCT) and dissociative ligand-field (LF) states in driving the photoinduced reactivity and suggest that the relative energies of these electronic states are tuned through modification of the supporting ligand. Our results are discussed in the context of developing new design principles that could be used to selectively control light-driven CO release from $[\text{Mn}(\text{CO})_3]$ complexes.

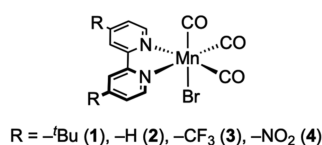
RESULTS AND DISCUSSION

Synthesis and Characterization. In order to study $[\text{Mn}(\text{CO})_3]$ complexes with uniformly tuned properties, we prepared compounds that differ only in the electron-donating/withdrawing nature of the substituents in the 4 and 4' positions of the supporting 2,2'-bipyridyl ligand. Complexes 1 and 2 were prepared according to prior reports,^{1,2} and the new derivatives 3 and 4 were synthesized and isolated using methods similar to those of Wrighton and co-workers (see the **Experimental Section** for details).⁴ Overall, no unusual features were encountered for the synthesized complexes. All of the formally manganese(I) complexes were prepared from $\text{Mn}(\text{CO})_5\text{Br}$ and isolated with inner-sphere bromide ligands. The compounds have C_s symmetry and are soluble in common organic solvents (e.g., MeCN, chloroform; see Figures S1–S5).

The $\text{Mn}(\text{CO})_3(^{\text{R}}\text{bpy})\text{Br}$ complexes have a variety of useful signatures that can be readily interrogated using NMR, IR, and electronic absorption spectroscopies. Trends in the spectra can be correlated with the ^Rbpy substituents using Hammett parameters.³⁰ However, the traditional Hammett parameter (σ) does not consider stabilization of partial or full charges in reference to inductive and resonance effects of the conjugated ligand. These limitations are accounted for in Brown's σ^+ parameter and Kubota's σ^- parameter, which stabilize partial or full positive and negative charges, respectively.^{31,32} To determine which parameter is most appropriate for a given system or spectroscopic signature, a series of Hammett plots are constructed to compare the goodness-of-fits with σ^+ , σ , and σ^- . For example, the ¹H NMR chemical shifts for the *o*-pyridyl protons of each complex correlate best with Brown's σ^+ parameter (see Figures S6 and S7), in agreement with prior literature.³³ The correlation with σ^+ indicates an inductive ground-state interaction between the ligand framework and substituents.

IR absorption spectroscopy confirms the presence of fac-tricarbonyl geometry for each of the complexes 1–4 in solution (see Figure S8) and demonstrates that the samples are free of $\text{Mn}(\text{CO})_5\text{Br}$ starting material (associated with absorption bands at 2004, 2046, and 2083 cm^{-1}). Our results from IR spectroscopy are consistent with previous observations of heteroleptic carbonyl complexes because we observe a systematic increase of the C–O stretching frequencies upon a change of the character of the 4,4'-substituents of ^Rbpy from electron donating to electron withdrawing.³⁴ Hammett plots of the A'' -symmetry C–O stretching frequency³⁵ as a function of the ligand substituent are best fit by the σ parameter ($R^2 = 0.993$), although the correlations with σ^+ ($R^2 = 0.989$) and σ^- ($R^2 = 0.945$) are not vastly different from the correlation with σ (see Figure S9). This observed correlation of C–O stretching frequencies is in agreement with the previous

Chart 1. $\text{Mn}(\text{CO})_3(^{\text{R}}\text{bpy})\text{Br}$ Complexes 1–4



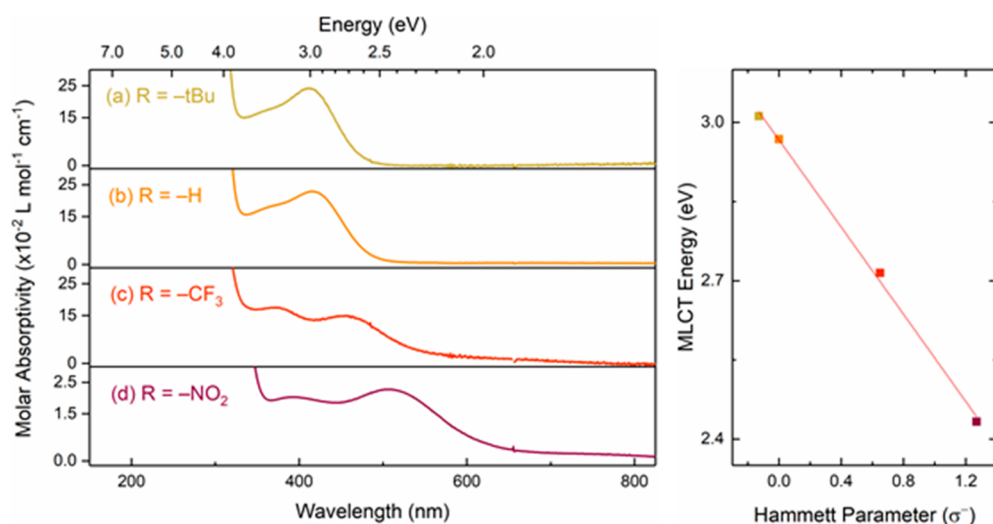


Figure 1. Electronic absorption spectra of **1–4** in MeCN (left). Hammett plot of the MLCT energy in electronvolts as a function of the σ^- parameter (right). The best-fit line in the Hammett plot reveals a correlation with $R^2 = 0.998$ and a slope of -0.41 ± 0.01 .

work on para-substituted isocyanide complexes $\text{CpFe}(\text{CO})_2(\text{CN}^R\text{Ph})$ and $\text{CpMn}(\text{CO})_2(\text{CN}^R\text{Ph})$, where Cp is cyclopentadienyl.^{36,37} However, because the C–O stretching modes are affected principally by π -bonding effects, the measured range of 15 cm^{-1} for the bipyridyl complexes under investigation here is consistent with the expected distal influence of the bipyridyl ligand substituents on the Mn metal center and the CO ligands.

Complexes **1–4** give vividly colored solutions when dissolved in common organic solvents like MeCN (see Figure S10). Figure 1 shows the electronic absorption spectra for all four complexes, and Table 1 lists the transition energies and

complexes featuring MLCT behavior.³⁹ A likely explanation for the decreasing transition strength with increasing electron-withdrawing character of the ligand substituents is reduced overlap of the HOMO and LUMO due to increased localization of the LUMO on the electron-withdrawing substituents. The electron-donating groups, in contrast, localize the LUMO closer to the Mn metal center, leading to better overlap with the HOMO and therefore a stronger MLCT transition. On the basis of this reasoning, the relatively weak transition for **4** follows the trend in the MLCT transition strengths set by the other three compounds, even though the lower absorption strength for **4** would typically be associated with a d–d transition. Although we cannot rule out the possibility of some d–d character in the lowest-energy transition for **4**, the strong correlation of both the transition energies and strengths with σ^- reinforces our assignment of the lowest-energy absorption bands as primarily MLCT in nature for all four compounds.

TA Spectroscopy. Ultrafast TA spectroscopy probes the reaction dynamics following MLCT excitation of the $[\text{Mn}(\text{CO})_3]$ complexes. On the basis of the shift of the MLCT bands with ligand substitution, we used excitation pulses at 420 nm for **1** and **2**, 470 nm for **3**, and 510 nm for **4**. Figure 2 shows the evolution of the TA spectra for **1–4** in MeCN. The initial excited-state absorption bands for compounds **1–3** are double-peaked and partially decay in $\leq 1 \text{ ps}$, followed by the delayed appearance of a narrower absorption band at slightly longer wavelength within $\sim 100 \text{ ps}$. The TA spectra are similar for all three compounds at longer time delays as well, except for a red shift of the TA bands that is similar to the shift of the ground-state MLCT bands across the three compounds. Notably, both the initial excited-state absorption bands and the new features that appear within $\sim 100 \text{ ps}$ follow the same trend as that of the ground-state MLCT bands of **1–3**, indicating that the ^Rbpy ligand remains bound to the Mn center for each of the TA species (see Figure S17).

The evolution of the TA spectrum for the nitro-disubstituted compound (**4**), also shown in Figure 2, is noticeably different from that for the other complexes. The initial excited-state absorption band is stronger and narrower and decays more slowly than that in the other compounds. Furthermore, no secondary absorption feature appears on the $\sim 100 \text{ ps}$ time

Table 1. Hammett Parameters of the Ligand Substituents and Selected Spectral Parameters for Complexes **1–4**

compound	Hammett parameter (σ^-)	λ (nm, eV)	ϵ ($\text{M}^{-1} \text{ cm}^{-1}$)
1	−0.13	412, 3.00	2426
2	0.0	415, 2.99	2288
3	0.65	457, 2.71	1502
4	1.27	510, 2.43	228

molar absorptivities for each of the lowest-energy absorption bands. Plotting the energies of the first absorption band for **1–4** as a function of the σ^- parameter gives an excellent correlation ($R^2 = 0.998$; see Figures S11–S15). On the basis of the molar absorptivity and a comparison with related compounds, the lowest-energy absorption bands for **1–4** can all be confidently assigned as having significant MLCT character (see Table 1). These findings agree with prior work on $\text{Mn}(\text{CO})_3(\text{diimine})\text{Br}$ complexes showing that the highest occupied molecular orbital (HOMO) is primarily localized on the Mn center, while the lowest unoccupied molecular orbital (LUMO) has significantly more ligand character, suggesting that the visible transitions are primarily MLCT in nature.³⁸ Plotting the molar absorptivity of the lowest-energy absorption bands of **1–4** as a function of the Hammett parameter also reveals a linear correlation with σ^- , where the transition strength increases for more electron-donating substituents (see Figure S16). Thus, the trend in the transition strength across all four compounds is roughly linear with σ^- , consistent with previous studies of transition-metal

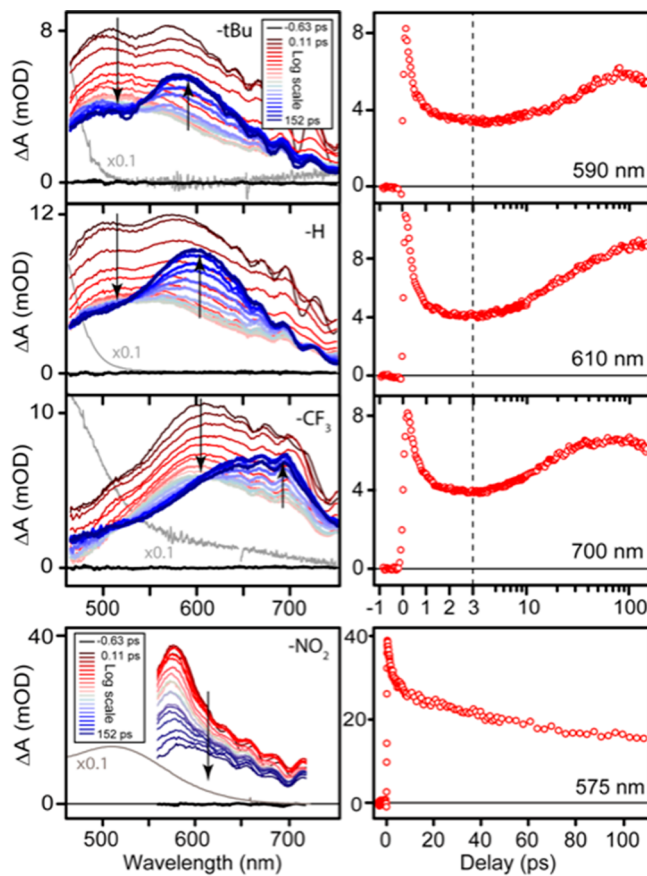
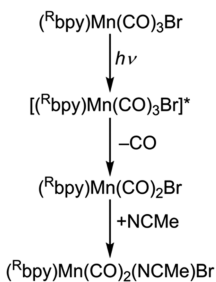


Figure 2. TA spectra of **1–4** (top to bottom) in MeCN. The left panel shows spectral evolution, and right panel shows the absorption change at a single wavelength. For reference, the ground-state absorption spectra are scaled by 0.1 and shown as gray lines.

scale in the TA spectrum of compound **4**. Unlike **1–3**, the shift in the wavelength of the initial TA band of **4** also does not follow the same trend as that of the ground-state MLCT bands. The strongly electron-withdrawing nitro groups likely localize the charge in the MLCT state, resulting in a more stable and longer-lived excited state for **4**.

On the basis of the TA spectroscopy and kinetics, as well as the observation of CO in the headspace of irradiated samples using GC analysis (see Figures S18 and S19), we propose a pathway for the early speciation process of complexes **1–3** that involves rapid CO loss followed by solvent coordination, as shown in Scheme 1. Optical excitation initially promotes an electron from a metal d orbital to the π^* orbital of the bpy ligand. The MLCT state is likely to be close in energy to a LF

Scheme 1. Proposed Mechanism for the Initial Pathway Leading to Speciation for Complexes **1–3**



state with d–d excitation on the metal that has significant antibonding (σ^*) character in the equatorial Mn–C bonds.⁴⁰ The antibonding LF state is stabilized by increasing the Mn–CO bond length, which results in a curve crossing that allows adiabatic population transfer from the MLCT state to the directly dissociative LF state (Figure 3). Impulsive release of a

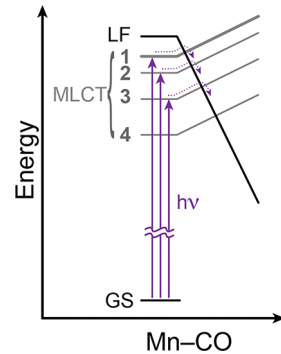


Figure 3. Schematic energy-level diagram illustrating how the change in Mn–CO bond length affects the curve crossing between the MLCT and LF states. The barrier for adiabatic population transfer increases with decreasing MLCT energy across the series **1–4** ($R = t\text{Bu, H, CF}_3, \text{NO}_2$).

CO ligand via the LF state generates an electron-deficient (16 e[−]), five-coordinate intermediate, $\text{Mn}(\text{CO})_2(\text{Rbpy})\text{Br}$. In MeCN, such an intermediate species is likely to bind a solvent ligand in order to recover a more stable 18 e[−] configuration. Thus, we attribute the new signal that rises on the tens of picoseconds time scale to the formation of a solvent-coordinated complex. Reduced electron back-bonding by the newly associated MeCN ligand compared with the CO that it replaces explains the red shift of the MLCT absorption bands of the solvent-coordinated complexes compared with the initial compounds.

A global fit to the TA spectrum of each compound using a biexponential function reveals the time constants for CO loss (τ_1) and solvent coordination (τ_2). The global fits give the time constants in Table 2 and the decay-associated spectra in

Table 2. Time Constants for CO Release (τ_1) and Solvent Coordination (τ_2)^a

compound	τ_1 (ps)	τ_2 (ps)
1	0.50 ± 0.10	39 ± 4
2	0.46 ± 0.10	30 ± 4
3	0.68 ± 0.20	18 ± 3

^aFrom global fits to the TA spectra for ~2 mM solutions of **1–3** in MeCN.

Figures S20–S22.⁴¹ The time constants indicate a slightly longer time scale for CO release and a shorter time scale for solvent coordination when the ligand becomes more electron-withdrawing. The trend in τ_2 is consistent with the formation of a relatively more electron-poor 16 e[−] complex in the case of the more electron-withdrawing ligand for **3**, compared with **2** and **1**.

In the proposed mechanism, the rate of CO loss is dependent on how quickly the MLCT state converts to the d–d dissociative LF state. Therefore, the observed rate of CO loss during photolysis likely depends on the initial relative energies of the MLCT and dissociative LF states. Changing the

substituents on the 4 and 4' positions of the bpy ligand should leave the metal d orbitals relatively unaffected while tuning the ligand π^* orbitals to a larger extent. The MLCT energy depends on π^* of the ligand, but the LF energy should be relatively insensitive to substitution, as illustrated in Figure 3. This picture is consistent with the trend that we observe in the time scales for CO loss in Table 2. Changing the substituents on the bpy ligand from electron donating to electron withdrawing stabilizes the MLCT state and therefore increases the barrier to reach the LF state (Figure 3). Accordingly, the increasing electron-withdrawing character of ${}^R\text{bpy}$ from 1 to 3 is associated with a corresponding decrease in the rate for CO loss (i.e., increase of τ_1) due to stabilization of the MLCT state and, therefore, a larger barrier-to-charge recombination by accessing the dissociative LF state.

As the substituents become even more electron-withdrawing, the π^* level of the bpy ligand is pushed substantially lower in energy compared with the occupied metal d orbitals. In the limiting case of the ${}^{\text{NO}_2}\text{bpy}$ complex (4), the MLCT band is >0.5 eV below that of the prototypical ${}^{\text{H}}\text{bpy}$ complex (2) due to charge stabilization and localization of the electron density on the nitro groups. Thus, the MLCT state of 4 is much lower than the dissociative LF state, significantly increasing the barrier for charge recombination and strongly disfavoring CO loss (see Figure S23). Instead, the MLCT state of 4 probably relaxes through a competing mechanism, possibly intersystem crossing to a triplet state that is relatively long-lived and persists beyond the time resolution of our experiment.

Measurement of CO Release by IR Spectroscopy. To confirm that the $[\text{Mn}(\text{CO})_3]$ complexes undergo CO loss followed by subsequent chemical reactivity in MeCN solvent, a series of photolysis experiments were carried out with IR spectroscopic monitoring to interrogate the generation of new species by irradiation of 2 with visible light. Following 2 min of irradiation with 415 nm light (at a total lamp power of 175 W), unique CO stretches appear in the IR spectrum, including stretches associated with manganese complexes between 2050 and 1825 cm^{-1} as well as the diagnostic stretch corresponding to free CO gas dissolved in MeCN near 2143 cm^{-1} (see Figure S24 for all spectra). Over time, the bands associated with 2 at 1924, 1934, and 2028 cm^{-1} decrease in intensity, and C–O stretches presumably associated with manganese-containing photoproducts grow in at 1883, 1961, and 1976 cm^{-1} ; two less intense features also appear at 1856 and 2050 cm^{-1} , but these features show minor variations in intensity over the 15 min irradiation time, suggesting that they may be associated with metastable intermediates. The presence of the $[\text{Mn}(\text{CO})_3(\text{bpy})]_2$ dimer can be inferred from related work examining electrochemical generation of the analogous $[\text{Mn}(\text{CO})_3({}^{\text{tBu}}\text{bpy})]_2$ dimer by Kubiak and co-workers.⁴² Because the speciation processes occurring at longer times are likely complex and multistep in nature, a portion of our future work will be devoted to further exploration by both time-resolved spectroscopies and more detailed steady-state photolysis experiments.

Involvement of MLCT versus LF States. Although the changing energy of the MLCT state with ligand substituents is evident from shifting of the ground-state absorption bands of 1–4, we have been unable to directly observe the relative energies of the LF states. The weak d–d transitions are not evident in the absorption spectra because of the stronger overlapping MLCT bands. We also attempted to measure the

d–d transition for the analogous bis(pyridine) complex, $\text{Mn}(\text{CO})_3\text{Br}(\text{py})_2$ (5), in an effort to determine the relative energy of the LF state in the $[\text{Mn}(\text{CO})_3]$ complexes (see Figure S25).

Although the synthesis of 5 was previously reported, the molecular structure of the complex was not reported. To obtain the structure, we grew single crystals of 5 suitable for X-ray diffraction (XRD) analysis by the vapor diffusion of diethyl ether into a concentrated MeCN solution (see Figures S26 and S27). Single crystals of the new complexes 3 and 4 suitable for XRD analysis were obtained with similar conditions (see Figures S28–S30). The expected atomic connectivity and fac-tricarbonyl geometry were confirmed in each case. While the donor strengths of py and bpy are similar (both molecules are conjugated imines with roughly the same electronic character), the average Mn–N bond distance in 5 [2.096(8) Å] is significantly longer than that found in the bipyridyl complexes 3 and 4 [2.051(4) and 2.039(6) Å, respectively], indicating a weaker interaction of the independent pyridyl rings in the $(\text{py})_2$ complex compared with bpy. Eliminating conjugation between the rings also pushes the π^* orbital of py to higher energy and shifts the MLCT band of 5 to shorter wavelength. However, even with the simultaneous blue shift of the MLCT band and weaker donation by pyridine, we do not observe a distinct d–d transition in the absorption spectrum of 5. On the other hand, it is interesting to note the presence of a shoulder band near 390 nm in the absorption spectra of all four diimine complexes (Figure 1), as well as 5; this band could be consistent with the presence of an overlapping d–d feature at higher energy than that of the observed lowest-energy MLCT bands.

Considering all of these features, the ultrafast TA results show that we can selectively control the sensitivity of the initial CO release by tuning the orbital energy levels of the $[\text{Mn}(\text{CO})_3\text{Br}({}^R\text{bpy})]$ complexes based on ligand substitution. Selectively controlling the loss of a CO ligand at the femtosecond time scale can lead to improved catalysts and more efficient photo-CORMs. On the one hand, preventing CO release would give more stable catalysts, and, on the other hand, complexes with tunable reactivity could serve as model compounds for regulating the therapeutic release of CO.

Secondary Reactivity following CO Loss. The CO release step is only the beginning of a more complex speciation process for these manganese complexes. After CO release in MeCN, the resulting electron-deficient five-coordinate species $[({}^R\text{bpy})\text{Mn}(\text{CO})_2\text{Br}]$ quickly binds a ligand to regain a full 18 e[−] valence. Table 2 shows that the time constants for solvent coordination (τ_2) decrease markedly as the ligand becomes more electron-withdrawing. Complexes with a more electron-deficient Mn center due to the electron-withdrawing ${}^{\text{CF}_3}\text{bpy}$ ligand (3) bind MeCN more quickly than the complexes bearing electron-donating ${}^{\text{tBu}}\text{bpy}$ (1) or ${}^{\text{H}}\text{bpy}$ ligands (2).

In order to test the solvent dependence of the secondary reactivity occurring upon CO loss, we also measured the evolution of the TA spectrum of 2 in chloroform (CHCl₃). Unlike MeCN, CHCl₃ is not generally considered to be a coordinating solvent.⁴³ Figure 4 shows that the evolution of the TA spectrum following MLCT excitation of 2 is very different in the two solvents. Specifically, the spectroscopic feature that appears on a picosecond time scale and is assigned as solvent coordination in MeCN is completely attenuated in CHCl₃, resulting in a broad and featureless spectrum that persists beyond the duration of our experiment.

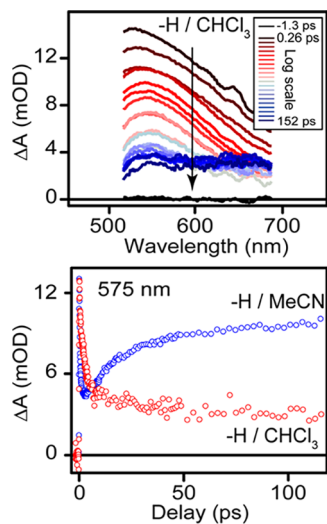


Figure 4. TA spectrum of **2** in CHCl₃ (upper panel) and a comparison of the kinetics at 575 nm for **2** in the coordinating solvent MeCN (blue markers) and in the noncoordinating solvent CHCl₃ (red markers).

In both cases of MeCN and CHCl₃ as the solvent, CO release exposes the coordinatively unsaturated, 16 e⁻ metal center to the solvent. Although direct solvent coordination is suppressed in CHCl₃, the electron-deficient, five-coordinate complex is likely to be susceptible to other bimolecular reactions, possibly including the oxidative addition of CHCl₃ or H-atom transfer from the solvent. The products from any of these reactions, or a combination of them, could be responsible for the broad, featureless TA spectrum that develops following excitation of **2** in CHCl₃. Indeed, the reactivity of this complex in CHCl₃ is consistent with recently reported TA measurements for manganese tetracarbonyl complexes supported by anionic chelating ligands.⁴⁴ However, regardless of the subsequent reactivity following solvent coordination, our results suggest that the feature that grows in at 100 ps in MeCN is likely a solvent-coordinated species, and this event can be controlled based on the choice of solvent.

CONCLUSIONS

Mn(CO)₃(^Rbpy)Br complexes are stable in the absence of light, which allowed us to extensively characterize them using a variety of techniques. Transitions in the NMR, IR, and electronic absorption spectra are linearly correlated with the Brown (σ^+), Hammett (σ), and Kubota (σ^-) parameters, respectively, providing insight into how ligand substituents govern electronic properties at the metal center. In the presence of light, Mn(CO)₃(^Rbpy)Br complexes **1–3** decompose via CO loss, with subsequent solvent coordination in MeCN or other reactions in CHCl₃. Ultrafast TA spectroscopy revealed the previously unknown five-coordinate and solvento-intermediates in the photospeciation process. Complex **4** follows a different reaction path that is likely the result of a long-lived triplet excited state that does not undergo decay to a dissociative LF (d-d) state. The different behavior of **1–4** illustrates how the reactivity and speciation of these complexes can be tuned by changing the electronic properties of the bidentate diimine ligand. Notably, because only limited computational modeling has been used to examine the excited-state electronic structure of Mn(CO)₃Br(diimine) complexes,^{38,45} further experimental work combined with

computational modeling would be useful in providing new insights into the speciation mechanisms operative during irradiation. Our ongoing experimental work aims to analyze the structure and electronics of the transient species generated upon irradiation using time-resolved X-ray absorption and IR spectroscopies.

EXPERIMENTAL SECTION

Potential Hazards. Working with carbonyl complexes poses a potential hazard of generating the colorless, odorless, tasteless, and acutely toxic gas CO. Work with carbonyl complexes should be carried out in a well-ventilated fume hood and with use of a sensitive CO monitor. The synthesis of complexes **1–5** involves the displacement of two CO ligands, resulting in the generation of a significant amount of CO during the reaction; this is especially true when working on larger scales (hundreds of milligrams), as has been done in the course of this work. Additionally, when complexes **1–5** are exposed to even low-intensity ambient visible light, they readily undergo photolysis to release CO. Caution should always be exercised when working with metal–carbonyl complexes.

General Considerations. Manganese pentacarbonyl bromide (98%, Beantown Chemical Co.), 2,2'-bipyridyl (bpy; 98%; Alfa Aesar), 4,4'-di-*tert*-butylbipyridine ('Bu-bpy; 98%, Sigma-Aldrich), 2-chloro-4-(trifluoromethyl)pyridine (98%; Oakwood Chemical), fuming nitric acid (90%, Alfa Aesar), and PCl₃ (98%, Alfa Aesar) were used as received. 2,2'-Bipyridyl *N,N'*-dioxide,⁴⁶ 4,4'-dinitro-2,2'-bipyridyl *N,N'*-dioxide,⁴⁶ 4,4'-dinitro-2,2'-bipyridyl (dnbp),⁴⁶ 4,4'-bis(trifluoromethyl)-2,2'-bipyridyl (CF₃-bpy),⁴⁷ Mn(CO)₃Br(pyridine)₂,⁴⁸ Mn(CO)₃Br(bpy),¹ and Mn(CO)₃Br[4,4'-bis(*tert*-butyl)-2,2'-bipyridyl]² were prepared according to literature methods with minor modifications. If necessary, the ligands bpy, 'Bu-bpy, and CF₃-bpy can be sublimed (at ca. 80 °C and 1 mTorr).

Deuterated NMR solvents were purchased from Cambridge Isotope Laboratories; CD₃CN was dried over molecular sieves. ¹H, ¹³C, and ¹⁹F NMR spectra were collected with 400 or 500 MHz Bruker spectrometers. Spectra were referenced to the residual protio solvent signal in the cases of ¹H and ¹³C NMR.⁴⁹ Heteronuclear NMR spectra were referenced to the appropriate external standard following the recommended scale based on the ratios of absolute frequencies (Ξ).⁵⁰ ¹⁹F NMR spectra are reported relative to CCl₃F. Chemical shifts (δ) are reported in units of parts per million, and coupling constants (J) are reported in hertz.

All manipulations were carried out in dry dinitrogen-filled gloveboxes (Vacuum Atmospheres Co. Hawthorne, CA) or under a dinitrogen atmosphere using standard Schlenk techniques unless otherwise noted. All solvents were of commercial grade, were dried over activated alumina using a Pure Process Technology (Nashua, NH) solvent purification system prior to use, and were stored over molecular sieves. All chemicals were from major commercial suppliers and were used as received after extensive drying.

IR spectra were collected on a PerkinElmer Spectrum 100 Fourier transform infrared spectrometer. UV-visible spectra were collected with an Ocean Optics FLAME-S spectrometer equipped with a DH-Mini light source. Steady-state photolysis experiments were carried out using an Oriel mercury–xenon arc lamp operating at 175 W and equipped with an Oriel Cornerstone 130 0.125 m monochromator accessory. For the experiments in which IR spectroscopic monitoring was used to examine the products of photolysis, an appropriate KBr plate cell was charged with a 17 mM solution of **2** in MeCN under an inert atmosphere, and an initial IR spectrum was collected prior to irradiation. Subsequent short periods of irradiation (totaling 2, 5, 10, and 15 min) with 415 nm light generated by the mercury–xenon arc lamp operating at 175 W were followed in each case by collection of a new spectrum in order to examine evolution of the system over time. These spectra are given in Figure S24.

Elemental analyses were performed by Midwest Microlab, Inc. (Indianapolis, IN).

Single-crystal diffraction data were collected with a Bruker Kappa APEX/II X-ray diffractometer. CCDC entries 1922040, 1922041, and

1922042 contain the supplementary crystallographic data for this paper.

The TA measurements used pump and probe pulses derived from the 800 nm output of a 1 kHz regeneratively amplified Ti:sapphire laser (Legend Elite, Coherent Inc., Santa Clara, CA). A portion of the laser fundamental pumped an optical parametric amplifier with two stages of nonlinear frequency conversion (TOPAS) to generate the visible pump pulses. The beam diameter at the sample was 160 μ m with an energy of 800 nJ/pulse. The relative polarization was set to a magic angle by rotating the pump pulses with a zero-order $\lambda/2$ waveplate. We used active background subtraction by passing the pump beam through a synchronized chopper wheel running at 500 Hz to block every other pump pulse. Broadband probe pulses with the desired wavelength range were generated by focusing a small fraction of the fundamental 800 nm laser light into a mechanically rotating CaF₂ crystal. The sample was cycled through a flow cell with a path length of 0.5 mm. After passing through the sample, the probe pulse was dispersed using a prism onto a 2069-element CCD array. Each TA spectrum was an average of 10³ laser pulses per time delay.

Synthesis of Mn(CO)₃[4,4'-bis(trifluoromethyl)-2,2'-bipyridine]Br (3). To a 50 mL Schlenk flask equipped with a stir bar was added 4,4'-bis(trifluoromethyl)-2,2'-bipyridine (0.0998 g, 0.342 mmol) in 50 mL of pentane. Then Mn(CO)₅Br (0.0890 g, 0.324 mmol) was added, and the reaction was brought to reflux under an argon atmosphere. The reaction was monitored by ¹H NMR until consumption of the starting material was observed (~6 h). Once the reaction had reached completion, the Schlenk flask was placed in a refrigerator at -20 °C for 30 min. The resulting solid was then filtered off with a fritted glass funnel and washed with cold pentane to afford the title compound as an orange-red solid. Yield: 0.0801 g (48%). ¹H NMR (400 MHz, CD₃CN): δ 9.48 (d, 2H, ³J_{H,H} = 5.8 Hz), 8.77 (s, 2H), 7.91 (dd, 2H, ³J_{H,H} = 5.8 Hz, ⁴J_{H,H} = 1.8 Hz). ¹³C{¹H} NMR (176 MHz, CD₃CN): δ 185.5, 157.5, 156.4, 141.2 (q, ¹J_{C,F} = 35.3 Hz), 124.8, 123.9 (q, ⁴J_{C,F} = 3.5 Hz), 122.6, 121.4 (q, ⁴J_{C,F} = 3.5 Hz). ¹⁹F NMR (376 MHz, CD₃CN): δ 65.4. Electronic absorption spectrum (MeCN): 208 (32000), 224 (33000), 293 (10000), 374 (1800), 454 nm (1500 M⁻¹ cm⁻¹). IR (THF): ν _{C=O} 2027 (m, A'), 1944 (m, A''), 1923 (m, A') cm⁻¹. ESI-MS (positive): *m/z* 471.9 (100%) (3 - Br⁻ + NCMe), 472.9 (23%), 474.0 (11%); 430.9 (87%) (3 - Br⁻), 431.9 (16%), 432.9 (2%); 429.0 (23%) (3 - Br⁻ - 3CO + 2NCMe), 430.0 (4%); 402.9 (17%) (3 - Br⁻ - CO), 403.9 (3%); 388.0 (20%) (3 - Br⁻ - 3CO + NCMe), 389.0 (4%); 374.9 (22%) (3 - Br⁻ - 2CO), 375.9 (4%); 346.9 (11%) (3 - Br⁻ - 3CO), 347.9 (2%) (see Figure S15). Anal. Calcd for MnC₁₅H₆BrF₆N₂O₃: C, 35.25; H, 1.18; N, 5.48. Found: C, 35.20; H, 1.24; N, 5.46.

Synthesis of Mn(CO)₃(dnbp)Br (4). To a Schlenk flask equipped with a stir bar was added 4,4'-dinitro-2,2'-bipyridine (0.3761 g, 1.53 mmol) and 50 mL of Et₂O. Then Mn(CO)₅Br (0.4005 g, 1.46 mmol) was added, and the reaction was brought to reflux under an argon atmosphere. The reaction was monitored by ¹H NMR until consumption of the starting material was observed (~12 h). Once the reaction had reached completion, the Schlenk flask was placed in a -20 °C refrigerator for 30 min. The resulting solid was then filtered off with a fritted glass funnel and washed with cold Et₂O to afford the title compound as a purple solid. Yield: 0.6409 g (95%). ¹H NMR (400 MHz, CD₃CN): δ 9.58 (d, 2H, ³J_{H,H} = 6.0 Hz), 9.21 (s, 2H), 8.29 (dd, 2H, ⁴J_{H,H} = 6.0 Hz). ¹³C{¹H} NMR (176 MHz, CD₃CN): δ 158.1, 157.1, 156.3, 120.5, 118.2. Electronic absorption spectrum (MeCN): 223 (1800), 245 (1400), 325 (800), 393 (200), 510 nm (230 M⁻¹ cm⁻¹). IR (THF): ν _{C=O} 2027 (m, A'), 1945 (m, A''), 1927 (m, A') cm⁻¹. ESI-MS (positive) *m/z* 425.9 (100%) (4 - Br⁻ + NCMe), 426.9 (17%), 427.9 (3%); 411.0 (31%) (4 - Br⁻ - 2CO + 2NCMe), 412.0 (6%), 413.0 (1%); 384.9 (9%) (4 - Br⁻), 385.9 (1%), 386.9 (1%); 383.0 (51%) (4 - Br⁻ - 3CO + 2NCMe), 384.0 (9%); 369.9 (7%) (4 - Br⁻ - 2CO + NCMe), 370.9 (1%), 372.0 (1%); 368.0 (20%) (4 - Br⁻ - CO - 2O + 2H + NCMe), 369.0 (3%) (see Figure S16). Anal. Calcd for MnC₁₃H₆BrN₄O₇ (+1H₂O): C, 32.32; H, 1.67; N, 11.60. Found: C, 32.52; H, 1.41; N, 11.67.

ASSOCIATED CONTENT

Supporting Information

The Supporting Information is available free of charge at <https://pubs.acs.org/doi/10.1021/acs.inorgchem.9b02758>.

NMR and IR spectra, crystallographic details, and electronic absorption spectra (PDF)
Cartesian coordinates (XYZ)

Accession Codes

CCDC 1922040-1922042 contain the supplementary crystallographic data for this paper. These data can be obtained free of charge via www.ccdc.cam.ac.uk/data_request/cif, or by emailing data_request@ccdc.cam.ac.uk, or by contacting The Cambridge Crystallographic Data Centre, 12 Union Road, Cambridge CB2 1EZ, UK; fax: +44 1223 336033.

AUTHOR INFORMATION

Corresponding Authors

Christopher G. Elles — Department of Chemistry, University of Kansas, Lawrence, Kansas 66045-7582, United States;
 orcid.org/0000-0002-1408-8360; Phone: +1 (785) 864-1922; Email: elles@ku.edu

James D. Blakemore — Department of Chemistry, University of Kansas, Lawrence, Kansas 66045-7582, United States;
 orcid.org/0000-0003-4172-7460; Phone: +1 (785) 864-3019; Email: blakemore@ku.edu

Authors

Wade C. Henke — Department of Chemistry, University of Kansas, Lawrence, Kansas 66045-7582, United States

Christopher J. Ootsuki — Department of Chemistry, University of Kansas, Lawrence, Kansas 66045-7582, United States

William N. G. Moore — Department of Chemistry, University of Kansas, Lawrence, Kansas 66045-7582, United States

Complete contact information is available at:
<https://pubs.acs.org/10.1021/acs.inorgchem.9b02758>

Author Contributions

[#]W.C.H. and C.J.O. contributed equally to this work. The manuscript was written with contributions from each of the listed authors. The final manuscript has been approved by all authors listed.

Notes

The authors declare no competing financial interest.

ACKNOWLEDGMENTS

The authors thank Dr. Davide Lionetti for numerous helpful discussions, Dr. Victor Day for assistance with X-ray crystallography, Keaton Prather for assistance with the preparation of 4,4'-dinitro-2,2'-bipyridine, and Prof. Misha Barybin for generous access to a benchtop IR spectrometer. This work was supported by the Hall Chemical Research Fund at the University of Kansas (to J.D.B. and C.G.E.) and a grant from the U.S. National Science Foundation (Grant CHE-1151555 to C.G.E.). W.C.H. was supported by the U.S. National Institutes of Health Graduate Training Program in the Dynamic Aspects of Chemical Biology (T32 GM008545-25).

REFERENCES

- (1) Bourrez, M.; Molton, F.; Chardon-Noblat, S.; Deronzier, A. [Mn(bipyridyl)(CO)₃Br]: An Abundant Metal Carbonyl Complex as

Efficient Electrocatalyst for CO₂ Reduction. *Angew. Chem., Int. Ed.* **2011**, *50*, 9903–9906.

(2) Smieja, J. M.; Sampson, M. D.; Grice, K. A.; Benson, E. E.; Froehlich, J. D.; Kubiak, C. P. Manganese as a Substitute for Rhenium in CO₂ Reduction Catalysts: The Importance of Acids. *Inorg. Chem.* **2013**, *52*, 2484–2491.

(3) Abel, E. W.; Bennett, M. A.; Wilkinson, G. Substituted carbonyl compounds of chromium, molybdenum, tungsten, and manganese. *J. Chem. Soc.* **1959**, 2323–2327.

(4) (a) Luong, J. C.; Faltynek, R. A.; Wrighton, M. S. Ground- and excited-state oxidation-reduction chemistry of (triphenyltin)- and (triphenylgermanium)tricarbonyl(1,10-phenanthroline)rhenium and related compounds. *J. Am. Chem. Soc.* **1980**, *102*, 7892–7900. (b) Caspar, J. V.; Meyer, T. J. Application of the energy gap law to nonradiative, excited-state decay. *J. Phys. Chem.* **1983**, *87*, 952–957. (c) Miguel, D.; Riera, V. Synthesis of manganese(I) carbonyls with σ -bonded alkynyl ligands. *J. Organomet. Chem.* **1985**, *293*, 379–390.

(5) (a) Hawecker, J.; Lehn, J. M.; Ziessel, R. Efficient photochemical reduction of CO₂ to CO by visible light irradiation of systems containing Re(bipy)(CO)₃X or Ru(bipy)₃²⁺–Co²⁺ combinations as homogeneous catalysts. *J. Chem. Soc., Chem. Commun.* **1983**, 536–538. (b) Hawecker, J.; Lehn, J. M.; Ziessel, R. Electrocatalytic reduction of carbon dioxide mediated by Re(bipy)(CO)₃Cl (bipy = 2,2'-bipyridine). *J. Chem. Soc., Chem. Commun.* **1984**, 328–330.

(6) (a) Sullivan, B. P.; Bolinger, C. M.; Conrad, D.; Vining, W. J.; Meyer, T. J. One- and two-electron pathways in the electrocatalytic reduction of CO₂ by fac-Re(bipy)(CO)₃Cl (bipy = 2,2'-bipyridine). *J. Chem. Soc., Chem. Commun.* **1985**, 1414–1416. (b) O'Toole, T. R.; Margerum, L. D.; Westmoreland, T. D.; Vining, W. J.; Murray, R. W.; Meyer, T. J. Electrocatalytic reduction of CO₂ at a chemically modified electrode. *J. Chem. Soc., Chem. Commun.* **1985**, 1416–1417.

(7) Fujita, E.; Hayashi, Y.; Kita, S.; Brunschwig, B. S. *Spectroscopic characterization of intermediates in CO₂ reduction with rhenium photocatalysts*; Elsevier: Amsterdam, The Netherlands, 2004; Vol. 153, pp 271–276.

(8) (a) Smieja, J. M.; Kubiak, C. P. Re(bipy-tBu)(CO)₃Cl–improved Catalytic Activity for Reduction of Carbon Dioxide: IR-Spectroelectrochemical and Mechanistic Studies. *Inorg. Chem.* **2010**, *49*, 9283–9289. (b) Clark, M. L.; Cheung, P. L.; Lessio, M.; Carter, E. A.; Kubiak, C. P. Kinetic and Mechanistic Effects of Bipyridine (bpy) Substituent, Labile Ligand, and Brønsted Acid on Electrocatalytic CO₂ Reduction by Re(bpy) Complexes. *ACS Catal.* **2018**, *8*, 2021–2029.

(9) Takeda, H.; Koike, K.; Morimoto, T.; Inumaru, H.; Ishitani, O. Photochemistry and photocatalysis of rhenium(I) diimine complexes. *Adv. Inorg. Chem.* **2011**, *63*, 137–186.

(10) El Nahhas, A.; van der Veen, R. M.; Penfold, T. J.; Pham, V. T.; Lima, F. A.; Abela, R.; Blanco-Rodriguez, A. M.; Záliš, S.; Vlček, A.; Tavernelli, I.; Rothlisberger, U.; Milne, C. J.; Chergui, M. X-ray Absorption Spectroscopy of Ground and Excited Rhenium–Carbonyl–Diimine Complexes: Evidence for a Two-Center Electron Transfer. *J. Phys. Chem. A* **2013**, *117*, 361–369.

(11) (a) Blakemore, J. D.; Gupta, A.; Warren, J. J.; Brunschwig, B. S.; Gray, H. B. Noncovalent Immobilization of Electrocatalysts on Carbon Electrodes for Fuel Production. *J. Am. Chem. Soc.* **2013**, *135*, 18288–18291. (b) Agarwal, J.; Shaw, T. W.; Stanton, C. J.; Majetich, G. F.; Bocarsly, A. B.; Schaefer, H. F. NHC-containing manganese(I) electrocatalysts for the two-electron reduction of CO₂. *Angew. Chem., Int. Ed.* **2014**, *53*, 5152–5155. (c) Grice, K. A.; Kubiak, C. P. Recent studies of rhenium and manganese bipyridine carbonyl catalysts for the electrochemical reduction of CO₂. *Adv. Inorg. Chem.* **2014**, *66*, 163–188. (d) Grills, D. C.; Farrington, J. A.; Layne, B. H.; Lymar, S. V.; Mello, B. A.; Preses, J. M.; Wishart, J. F. Mechanism of the Formation of a Mn-Based CO₂ Reduction Catalyst Revealed by Pulse Radiolysis with Time-Resolved Infrared Detection. *J. Am. Chem. Soc.* **2014**, *136*, 5563–5566. (e) Sampson, M. D.; Nguyen, A. D.; Grice, K. A.; Moore, C. E.; Rheingold, A. L.; Kubiak, C. P. Manganese catalysts with bulky bipyridine ligands for the electrocatalytic reduction of carbon dioxide: Eliminating dimerization and altering catalysis. *J. Am. Chem. Soc.* **2014**, *136*, 5460–5471. (f) Walsh, J. J.; Neri, G.; Smith, C. L.; Cowan, A. J. Electrocatalytic CO₂ reduction with a membrane supported manganese catalyst in aqueous solution. *Chem. Commun.* **2014**, *50*, 12698–12701. (g) Zeng, Q.; Tory, J.; Hartl, F. Electrocatalytic Reduction of Carbon Dioxide with a Manganese(I) Tricarbonyl Complex Containing a Nonaromatic α -Diimine Ligand. *Organometallics* **2014**, *33*, 5002–5008.

(12) (a) Agarwal, J.; Shaw, T. W.; Schaefer, H. F., III; Bocarsly, A. B. Design of a Catalytic Active Site for Electrochemical CO₂ Reduction with Mn(I)-Tricarbonyl Species. *Inorg. Chem.* **2015**, *54*, 5285–5294. (b) Fei, H.; Sampson, M. D.; Lee, Y.; Kubiak, C. P.; Cohen, S. M. Photocatalytic CO₂ Reduction to Formate Using a Mn(I) Molecular Catalyst in a Robust Metal-Organic Framework. *Inorg. Chem.* **2015**, *54*, 6821–6828. (c) Machan, C. W.; Stanton, C. J., III; Vandezande, J. E.; Majetich, G. F.; Schaefer, H. F., III; Kubiak, C. P.; Agarwal, J. Electrocatalytic Reduction of Carbon Dioxide by Mn(CN)(2,2'-bipyridine)(CO)₃: CN Coordination Alters Mechanism. *Inorg. Chem.* **2015**, *54*, 8849–8856. (d) Riplinger, C.; Carter, E. A. Influence of Weak Brønsted Acids on Electrocatalytic CO₂ Reduction by Manganese and Rhenium Bipyridine Catalysts. *ACS Catal.* **2015**, *5*, 900–908. (e) Walsh, J. J.; Smith, C. L.; Neri, G.; Whitehead, G. F. S.; Robertson, C. M.; Cowan, A. J. Improving the efficiency of electrochemical CO₂ reduction using immobilized manganese complexes. *Faraday Discuss.* **2015**, *183*, 147–160. (f) Agnew, D. W.; Sampson, M. D.; Moore, C. E.; Rheingold, A. L.; Kubiak, C. P.; Figueroa, J. S. Electrochemical Properties and CO₂-Reduction Ability of m-Terphenyl Isocyanide Supported Manganese Tricarbonyl Complexes. *Inorg. Chem.* **2016**, *55*, 12400–12408. (g) Rawat, K. S.; Mahata, A.; Choudhuri, I.; Pathak, B. N-Heterocyclic Carbene-Based Mn Electrocatalyst for Two-Electron CO₂ Reduction over Proton Reduction. *J. Phys. Chem. C* **2016**, *120*, 8821–8831.

(13) (a) Sampson, M. D.; Kubiak, C. P. Manganese Electrocatalysts with Bulky Bipyridine Ligands: Utilizing Lewis Acids To Promote Carbon Dioxide Reduction at Low Overpotentials. *J. Am. Chem. Soc.* **2016**, *138*, 1386–1393. (b) Spall, S. J. P.; Keane, T.; Tory, J.; Cocker, D. C.; Adams, H.; Fowler, H.; Meijer, A. J. H. M.; Hartl, F.; Weinstein, J. A. Manganese Tricarbonyl Complexes with Asymmetric 2-Iminopyridine Ligands: Toward Decoupling Steric and Electronic Factors in Electrocatalytic CO₂ Reduction. *Inorg. Chem.* **2016**, *55*, 12568–12582. (c) Stanton, C. J.; Vandezande, J. E.; Majetich, G. F.; Schaefer, H. F.; Agarwal, J. Mn-NHC Electrocatalysts: Increasing π Acidity Lowers the Reduction Potential and Increases the Turnover Frequency for CO₂ Reduction. *Inorg. Chem.* **2016**, *55*, 9509–9512. (d) Ngo, K. T.; McKinnon, M.; Mahanti, B.; Narayanan, R.; Grills, D. C.; Ertem, M. Z.; Rochford, J. Turning on the Protonation-First Pathway for Electrocatalytic CO₂ Reduction by Manganese Bipyridyl Tricarbonyl Complexes. *J. Am. Chem. Soc.* **2017**, *139*, 2604–2618. (e) Reuillard, B.; Ly, K. H.; Rosser, T. E.; Kuehnel, M. F.; Zebger, I.; Reisner, E. Tuning Product Selectivity for Aqueous CO₂ Reduction with a Mn(bipyridine)-pyrene Catalyst Immobilized on a Carbon Nanotube Electrode. *J. Am. Chem. Soc.* **2017**, *139*, 14425–14435. (f) Franco, F.; Pinto, M. F.; Royo, B.; Lloret-Fillol, J. A Highly Active N-Heterocyclic Carbene Manganese(I) Complex for Selective Electrocatalytic CO₂ Reduction to CO. *Angew. Chem., Int. Ed.* **2018**, *57*, 4603–4606. (g) Myren, T. H. T.; Lilio, A. M.; Huntzinger, C. G.; Horstman, J. W.; Stinson, T. A.; Donadt, T. B.; Moore, C.; Lama, B.; Funke, H. H.; Luca, O. R. Manganese N-Heterocyclic Carbene Pincers for the Electrocatalytic Reduction of Carbon Dioxide. *Organometallics* **2019**, *38*, 1248–1253. (h) Takeda, H.; Kamiyama, H.; Okamoto, K.; Irimajiri, M.; Mizutani, T.; Koike, K.; Sekine, A.; Ishitani, O. Highly Efficient and Robust Photocatalytic Systems for CO₂ Reduction Consisting of a Cu(I) Photosensitizer and Mn(I) Catalysts. *J. Am. Chem. Soc.* **2018**, *140*, 17241–17254. (i) Tignor, S. E.; Kuo, H.-Y.; Lee, T. S.; Scholes, G. D.; Bocarsly, A. B. Manganese-Based Catalysts with Varying Ligand Substituents for the Electrochemical Reduction of CO₂ to CO. *Organometallics* **2019**, *38*, 1292–1299. (j) Walsh, J. J.; Neri, G.; Smith, C. L.; Cowan, A. J. Water-Soluble Manganese Complex for Selective Electrocatalytic CO₂ Reduction to CO. *Organometallics* **2019**, *38*, 1224–1229.

(14) Vollmer, M. V.; Machan, C. W.; Clark, M. L.; Antholine, W. E.; Agarwal, J.; Schaefer, H. F.; Kubiak, C. P.; Walensky, J. R. Synthesis, Spectroscopy, and Electrochemistry of (α -Diimine)M(CO)₃Br, M = Mn, Re, Complexes: Ligands Isoelectronic to Bipyridyl Show Differences in CO₂ Reduction. *Organometallics* **2015**, *34*, 3–12.

(15) Takeda, H.; Koizumi, H.; Okamoto, K.; Ishitani, O. Photocatalytic CO₂ reduction using a Mn complex as a catalyst. *Chem. Commun.* **2014**, *50*, 1491–1493.

(16) Agarwal, J.; Stanton, C. J., III; Shaw, T. W.; Vandezande, J. E.; Majetich, G. F.; Bocarsly, A. B.; Schaefer, H. F., III Exploring the effect of axial ligand substitution (X = Br, NCS, CN) on the photodecomposition and electrochemical activity of [MnX(N-C)(CO)₃] complexes. *Dalton Trans.* **2015**, *44*, 2122–2131.

(17) Perutz, R. N.; Torres, O.; Vlček, A. Photochemistry of Metal Carbonyls. In *Comprehensive Inorganic Chemistry II*, 2nd ed.; Reedijk, J., Poepelmeier, K., Eds.; Elsevier: Amsterdam, The Netherlands, 2013; Vol. 8.

(18) (a) Schatzschneider, U. PhotoCORMs: Light-triggered release of carbon monoxide from the coordination sphere of transition metal complexes for biological applications. *Inorg. Chim. Acta* **2011**, *374*, 19–23. (b) Kottelat, E.; Fabio, Z. Visible Light Activated PhotoCORMs. *Inorganics* **2017**, *5*, 24. (c) Ling, K.; Men, F.; Wang, W.-C.; Zhou, Y.-Q.; Zhang, H.-W.; Ye, D.-W. Carbon Monoxide and Its Controlled Release: Therapeutic Application, Detection, and Development of Carbon Monoxide Releasing Molecules (CORMs). *J. Med. Chem.* **2018**, *61*, 2611–2635.

(19) (a) Hughey, J. L.; Anderson, C. P.; Meyer, T. J. Photochemistry of Mn₂(CO)₁₀. *J. Organomet. Chem.* **1977**, *125*, C49–C52. (b) Meyer, T. J.; Caspar, J. V. Photochemistry of metal-metal bonds. *Chem. Rev.* **1985**, *85*, 187–218.

(20) Motterlini, R.; Clark, J. E.; Foresti, R.; Sarathchandra, P.; Mann, B. E.; Green, C. J. Carbon Monoxide-Releasing Molecules: Characterization of Biochemical and Vascular Activities. *Circ. Res.* **2002**, *90*, e17–e24.

(21) Bolze, F.; Jenni, S.; Sour, A.; Heitz, V. Molecular photosensitisers for two-photon photodynamic therapy. *Chem. Commun.* **2017**, *53*, 12857–12877.

(22) Niesel, J.; Pinto, A.; Peindy N'Dongo, H. W.; Merz, K.; Ott, I.; Gust, R.; Schatzschneider, U. Photoinduced CO release, cellular uptake and cytotoxicity of a tris(pyrazolyl)methane (tpm) manganese tricarbonyl complex. *Chem. Commun.* **2008**, 1798–1800.

(23) (a) He, Q.; Kiesewetter, D. O.; Qu, Y.; Fu, X.; Fan, J.; Huang, P.; Liu, Y.; Zhu, G.; Liu, Y.; Qian, Z.; Chen, X. NIR-Responsive On-Demand Release of CO from Metal Carbonyl-Caged Graphene Oxide Nanomedicine. *Adv. Mater.* **2015**, *27*, 6741–6746. (b) Ruggi, A.; Zobi, F. Quantum-CORMs: quantum dot sensitized CO releasing molecules. *Dalton Trans.* **2015**, *44*, 10928–31. (c) Autcott, B. J.; Ward, J. S.; Andrew, S. G.; Milani, J.; Whitwood, A. C.; Lynam, J. M.; Parkin, A.; Fairlamb, I. J. S. Redox-tagged carbon monoxide-releasing molecules (CORMs): ferrocene-containing [Mn(C-N)(CO)₄] complexes as a promising new CORM class. *Inorg. Chem.* **2017**, *56*, 5431–5440. (d) Carmona, F. J.; Jimenez-Amezcu, I.; Rojas, S.; Romao, C. C.; Navarro, J. A. R.; Maldonado, C. R.; Barea, E. Aluminum Doped MCM-41 Nanoparticles as Platforms for the Dual Encapsulation of a CO-Releasing Molecule and Cisplatin. *Inorg. Chem.* **2017**, *56*, 10474–10480. (e) Li, Z.; Pierri, A. E.; Huang, P.-J.; Wu, G.; Iretskii, A. V.; Ford, P. C. Dinuclear PhotoCORMs: Dioxygen-Assisted Carbon Monoxide Uncaging from Long-Wavelength-Absorbing Metal–Metal-Bonded Carbonyl Complexes. *Inorg. Chem.* **2017**, *56*, 6094–6104. (f) Mansour, A. M. Rapid green and blue light-induced CO release from bromazepam Mn(I) and Ru(II) carbonyls: synthesis, density functional theory and biological activity evaluation. *Appl. Organomet. Chem.* **2017**, *31*, No. e3564. (g) Mede, R.; Hoffmann, P.; Klein, M.; Goerls, H.; Schmitt, M.; Neugebauer, U.; Gessner, G.; Heinemann, S. H.; Popp, J.; Westerhausen, M. Water-Soluble Mn(CO)₃-Based and Non-Toxic PhotoCORM for Administration of Carbon Monoxide Inside of Cells. *Z. Anorg. Allg. Chem.* **2017**, *643*, 2057–2062. (h) Reddy, G. U.; Liu, J.; Steinmetzer, J.; Grafe, S.; Gorls, H.; Kupfer, S.; Askes, S. H. C.; Neugebauer, U.; Grafe, S.; Schiller, A. Light-responsive paper strips as CO-releasing material with a colourimetric response. *Chem. Sci.* **2017**, *8*, 6555–6560. (i) Mansour, A. M.; Shehab, O. R. Reactivity of visible-light induced CO releasing thiourea-based Mn(I) tricarbonyl bromide (CORM-NS1) towards lysozyme. *Inorg. Chim. Acta* **2018**, *480*, 159–165.

(24) Carrington, S. J.; Chakraborty, I.; Mascharak, P. K. Exceptionally rapid CO release from a manganese(I) tricarbonyl complex derived from bis(4-chloro-phenylimino)acenaphthene upon exposure to visible light. *Dalton Trans.* **2015**, *44*, 13828–13834.

(25) Glyn, P.; George, M. W.; Hodges, P. M.; Turner, J. J. Fast time-resolved IR studies of the excited states of co-ordination compound: direct observation of intramolecular charge transfer. *J. Chem. Soc., Chem. Commun.* **1989**, 1655–1657.

(26) Sato, S.; Matubara, Y.; Koike, K.; Falkenström, M.; Katayama, T.; Ishibashi, Y.; Miyasaka, H.; Taniguchi, S.; Chosrowjan, H.; Mataga, N.; Fukazawa, N.; Koshihara, S.; Onda, K.; Ishitani, O. Photochemistry of fac-[Re(bpy)(CO)₃Cl]. *Chem. - Eur. J.* **2012**, *18*, 15722–15734.

(27) Stufkens, D. J.; Vlček, A. Ligand-dependent excited state behaviour of Re(I) and Ru(II) carbonyl-diimine complexes. *Coord. Chem. Rev.* **1998**, *177*, 127–179.

(28) (a) Cannizzo, A.; Blanco-Rodriguez, A. M.; El Nahhas, A.; Sebera, J.; Zalis, S.; Vlček, A.; Chergui, M. Femtosecond Fluorescence and Intersystem Crossing in Rhenium(I) Carbonyl–Bipyridine Complexes. *J. Am. Chem. Soc.* **2008**, *130*, 8967–8974. (b) El Nahhas, A.; Consani, C.; Blanco-Rodriguez, A. M.; Lancaster, K. M.; Braem, O.; Cannizzo, A.; Townie, M.; Clark, I. P.; Zalis, S.; Chergui, M.; Vlček, A. Ultrafast Excited-State Dynamics of Rhenium(I) Photosensitizers [Re(Cl)(CO)₃(N,N)]⁺ and [Re(imidazole)-(CO)₃(N,N)]⁺: Diimine Effects. *Inorg. Chem.* **2011**, *50*, 2932–2943.

(29) Grills, D. C.; Farrington, J. A.; Layne, B. H.; Lyman, S. V.; Mello, B. A.; Preses, J. M.; Wishart, J. F. Mechanism of the Formation of a Mn-Based CO₂ Reduction Catalyst Revealed by Pulse Radiolysis with Time-Resolved Infrared Detection. *J. Am. Chem. Soc.* **2014**, *136*, 5563–5566.

(30) Hammett, L. P. The Effect of Structure upon the Reactions of Organic Compounds. Benzene Derivatives. *J. Am. Chem. Soc.* **1937**, *59*, 96–103.

(31) Brown, H. C.; Okamoto, Y. Electrophilic Substituent Constants. *J. Am. Chem. Soc.* **1958**, *80*, 4979–4987.

(32) Yoshioka, M.; Hamamoto, K.; Kubota, T. Relationship between Acid and Dissociation Constants of N1-Aryl-sulfonilamides and the Hammett Equation. *Bull. Chem. Soc. Jpn.* **1962**, *35*, 1723–1728.

(33) von Philipsborn, W. Probing organometallic structure and reactivity by transition metal NMR spectroscopy. *Chem. Soc. Rev.* **1999**, *28*, 95–105.

(34) Hoye, T. R.; Rehberg, G. M. Reactions of (CO)₅Cr:C(Me)-N(CH₂CH₂)₂ with enynes: mechanistic insight and synthetic value of changing a carbene donor group from alkoxy to dialkylamino. *Organometallics* **1989**, *8*, 2070–2071.

(35) Stor, G. J.; Morrison, S. L.; Stufkens, D. J.; Oskam, A. The Remarkable Photochemistry of *fac*-XMn(CO)₃(α -diimine) (X = Halide): Formation of Mn₂(CO)₆(α -diimine)₂ via the mer Isomer and Photocatalytic Substitution of X- in the Presence of PR₃. *Organometallics* **1994**, *13*, 2641–2650.

(36) Zimmer, P.; Sun, Y.; Thiel, W. R. Cationic isonitrile complexes of the CpFe(CO)₂ fragment. *J. Organomet. Chem.* **2014**, *774*, 12–18.

(37) Herberhold, M.; Brabetz, H. Übergangsmetallkomplexe mit N-haltigen Liganden, III. Donator-Akzeptor-Eigenschaften organischer Nitrile im System C₅H₅Mn(CO)₂L. *Chem. Ber.* **1970**, *103*, 3909–3917.

(38) Jiang, Q.; Xia, Y.; Barrett, J.; Mikhailovsky, A.; Wu, G.; Wang, D.; Shi, P.; Ford, P. C. Near-Infrared and Visible Photoactivation to Uncage Carbon Monoxide from an Aqueous-Soluble PhotoCORM. *Inorg. Chem.* **2019**, *58*, 11066–11075.

(39) Papadakis, R.; Tsolomitis, A. Study of the correlations of the MLCT Vis absorption maxima of 4-pentacyanoferrate- 4'-aryl-substituted bispyridinium complexes with the Hammett substituent

parameters and the solvent polarity parameters E and AN. *J. Phys. Org. Chem.* **2009**, *22*, 515–521.

(40) Hummel, P.; Oxgaard, J.; Goddard, W. A.; Gray, H. B. Ligand-Field Excited States of Metal Hexacarbonyls. *Inorg. Chem.* **2005**, *44*, 2454–2458.

(41) van Stokkum, I. H. M.; Larsen, D. S.; van Grondelle, R. Global and target analysis of time-resolved spectra. *Biochim. Biophys. Acta, Bioenerg.* **2004**, *1657*, 82–104.

(42) Machan, C. W.; Sampson, M. D.; Chabolla, S. A.; Dang, T.; Kubiak, C. P. developing a mechanistic understanding of molecular electrocatalysts for CO₂ reduction using infrared spectroelectrochemistry. *Organometallics* **2014**, *33*, 4550–4559.

(43) Díaz-Torres, R.; Alvarez, S. Coordinating ability of anions and solvents towards transition metals and lanthanides. *Dalton Trans.* **2011**, *40*, 10742–10750.

(44) Hammarback, L. A.; Clark, I. P.; Sazanovich, I. V.; Towrie, M.; Robinson, A.; Clarke, F.; Meyer, S.; Fairlamb, I. J. S.; Lynam, J. M. Mapping out the key carbon–carbon bond-forming steps in Mn-catalysed C–H functionalization. *Nature Catalysis* **2018**, *1*, 830–840.

(45) Mansour, A. M.; Ragab, M. S. Spectroscopic and DFT studies of photoactivatable Mn(I) tricarbonyl complexes. *Appl. Organomet. Chem.* **2019**, *33*, No. e4944.

(46) Maerker, G.; Case, F. H. The Synthesis of Some 4,4'-Disubstituted 2,2'-Bipyridines. *J. Am. Chem. Soc.* **1958**, *80*, 2745–2748.

(47) Li, H.; Oppenheimer, J.; Smith, M. R., III; Maleczka, R. E., Jr Improved synthesis of electron deficient bipyridines. *Tetrahedron Lett.* **2016**, *57*, 2231–2232.

(48) Pons, M.; Herberich, G.; Kirk, P. N.; Castellani, M. P.; Rizzo, M. J.; Atwood, J. D. Bromotricarbonyl-di(pyridine)manganese(I). *Inorg. Synth.* **2014**, *36*, 148–149.

(49) Fulmer, G. R.; Miller, A. J. M.; Sherden, N. H.; Gottlieb, H. E.; Nudelman, A.; Stoltz, B. M.; Bercaw, J. E.; Goldberg, K. I. NMR Chemical Shifts of Trace Impurities: Common Laboratory Solvents, Organics, and Gases in Deuterated Solvents Relevant to the Organometallic Chemist. *Organometallics* **2010**, *29*, 2176–2179.

(50) (a) Harris, R. K.; Becker, E. D.; Cabral De Menezes, S. M.; Goodfellow, R.; Granger, P. NMR nomenclature. Nuclear spin properties and conventions for chemical shifts (IUPAC Recommendations 2001). *Pure Appl. Chem.* **2001**, *73*, 1795–1818. (b) Harris, R. K.; Becker, E. D.; Cabral De Menezes, S. M.; Granger, P.; Hoffman, R. E.; Zilm, K. W. Further Conventions for NMR Shielding and Chemical Shifts (IUPAC Recommendations 2008). *Pure Appl. Chem.* **2008**, *80*, 59–84.